Handling Qualities Analysis of Blade Pitch and Rotor Speed Controlled eVTOL Quadrotor Concepts for Urban Air Mobility

Carlos Malpica
carlos.a.malpica@nasa.gov
Aerospace Engineer
NASA Ames Research Center
Moffett Field, CA

Shannah Withrow-Maser
shannah.n.withrow@nasa.gov
Aerospace Engineer
NASA Ames Research Center
Moffett Field, CA

ABSTRACT

A study of the handling qualities of quadrotor designs for urban air mobility (UAM) application was performed. Eight different quadrotor configurations based on NASA reference concept vehicles were considered for investigation. The study was based on NASA single-passenger (250-lb payload) 50-nm range and six-passenger (1,200-lb payload) reference quadrotor designs. Intermediate-sized two- and four-passenger (400- and 800-lb payload) designs formed the final candidate configurations. All aircraft were equipped with electric motors for propulsion, but different variants were configured with variable pitch (collective) control (with constant rotor speed) or variable rotor speed control (with constant pitch). Flight dynamics models developed had sufficient richness of detail to conduct flight control or handling qualities assessments. Based on the various modeling assumptions, assessments showed that collective control was feasible, whereas rotor speed-based control exhibited unstable closed-loop roll and pitch dynamics. Vehicle size in the range considered did not cause significant change in the handling qualities because of a fundamental trade-off between the underlying parameters that govern the control power-to-weight (inertia) ratio.

NOTATION

A	Bare-airframe stability derivative matrix
B	Motor friction and viscous losses coefficient
B	Bare-airframe control derivative matrix
c	Torque SI unit conversion constant (0.7374 lb-ft/Nm)
C	Bare-airframe state output matrix
D	Bare-airframe control output matrix
D_e	Motor rotor external diameter (ft)
f_d	Drive system inertia factor
H_s	Rotor speed sensor transfer function
i_a	Motor armature current (A)
I	Trim value of the motor armature current (A)
I_r	Main rotor rotational moment of inertia (slug ft^2)
J	Drive system rotational moment of inertia (slug ft^2)
K_e	Motor back-EMF constant (Vs)
K_m	Motor torque constant (slug ft^2), $K_m = cK_e$
L_a	Motor armature inductance (H or μH)
M	Motor rotational mass (slug)
N_s	Number of battery cells in series
N_{spec}	Specification propulsion group engine speed (rpm or rad/s)
Q_A	Rotor aerodynamic torque (lb-ft)
Q_S	Rotor shaft torque (lb-ft)
p	Roll rate (deg/s)
P_{eng}	Sea level static (SLS) power available per engine at specified takeoff rating (hp)
q	Pitch rate (deg/s)
r	Yaw rate (deg/s)
r	Drive system gear ratio
R	Main rotor radius (ft)
R_a	Motor armature resistance (Ω)
s	Laplace domain variable (rad/s)
t	Time (s)
T_c	Motor natural response time constant (s)
T_{mix}	Control system command mixing matrix (rad/s/in)
u	Body-axis longitudinal velocity (ft/s)
v	Body-axis lateral velocity (ft/s)
V	Voltage (V)
V_a	Motor armature voltage input (V)
V_{ref}	Battery cell reference voltage (V)
w	Body-axis heave velocity (ft/s)
x_{mbd}	Battery maximum burst discharge rate
η	Motor efficiency factor
λ	Inductance proportionality constant
ϕ	Euler body-axis roll attitude angle (deg)
θ	Euler body-axis pitch attitude angle (deg)
ψ	Euler body-axis yaw attitude angle (deg)
τ	Motor torque (lb-ft)
ω	Motor speed (rad/s)
Ω	Main rotor speed (rad/s)
Ω_{cmd}	Main rotor speed controller command (rad/s)
$\dot{\Omega}$	Main rotor acceleration (rad/s^2)

Presented at the VFS International Powered Lift Conference 2020, San Jose, CA, January 21–23, 2020.

INTRODUCTION

Many concepts for urban air mobility (UAM) employ all-electric, speed-controlled rotors, similar to those widely used in the drone industry. An alternative to traditional collective and cyclic control, these designs, if viable, could reduce weight and complexity. Vehicle design and performance trade-offs between the two control concepts were explored in

Ref. 1. The influence of various propulsion technologies on vehicle size was investigated on six-passenger quadrotor, lift+cruise and side-by-side VTOL concepts designed to a common sizing mission profile (Ref. 2). In that study authors presumed that rotor speed control would be unlikely for the quadrotor design, because of the large size of the quadrotor rotors. Thus, it is necessary to determine the control and handling qualities limitations that result from scaling these concepts to much larger passenger vehicles (Ref. 3). Controls tools which have been used for previous analyses by the NASA Ames Aeromechanics Branch had not been configured for all-electric vehicles. For example, motors, previously modeled as actuators, must be replaced with a representative, yet simple, model of the motor drive system that is functionally related to the vehicle sizing. Improved models of rotor speed-controlled configurations will allow researchers to more comprehensively assess the viability of speed-controlled designs. The aim of this study is to assess, at the conceptual design level, the performance of variable speed and variable pitch rotor configurations in terms of handling qualities such as small-amplitude attitude bandwidth and phase delay of a vehicle sized for UAM applications. Electric, collective-controlled models will also be assessed for feasibility and as an alternative, if needed, to speed-controlled models. Additionally, the vehicles will be sized to various passenger capacities (payloads) in order to determine how the size of the vehicle affects handling qualities. Figure 1 illustrates the existing NASA single- and six-passenger reference quadcopter concept designs.

(a)

(b)

Figure 1. Artist renderings of NASA reference quadrotor configurations: a) single-passenger, and b) six-passenger

Previous assessment of multirotor control systems, especially variable speed-controlled models has been performed primarily on small scale UAVs such as would potentially be used for surveillance, package delivery, etc., opposed to multirotor configurations sized for passengers. Saetti et al. describes an Explicit Model Following (EMF) controller and Dynamic Inversion (DI) controller created for a small COTS quadcopter, including the robustness of the models (Ref. 4). Ivler et al. discusses dynamic response scaling for such vehicles in order to determine proper control system design and handling qualities methods (currently limited to multirotors in the same size class) (Ref. 5). Long term, the authors intend to extend this research to include larger, passenger sized vehicles. The analysis described below is the first step in creating such models. This analysis will be complemented by a future Vertical Motion Simulator (VMS) test that will provide experimental data to support analysis of these larger vehicle configurations and control systems.

Much of the current UAM research has focused on power and propulsion systems. One exception is the Lombaerts, et. al study, which used Nonlinear Dynamic Inversion (NDI) and Incremental Nonlinear Dynamic Inversion (INDI) methods, to design controllers for a passenger-sized eVTOL Quad Tiltrotor and assess some handling qualities implications (Ref. 6). Contributors to this research are also collaborators for the planned eVTOL quadrotor VMS test.

TECHNICAL APPROACH

Central to this study is refining a process by which the relevant flight dynamics of eVTOL multirotor configurations (quadrotors in this instance) can be systematically modeled from parameters that flow from conceptual design analysis. This point is crucial to the mapping of the flight control or handling qualities analysis to vehicle design, so as to be able to unravel the potentially complex parameter interrelations.

Analysis Tools

Hover bare-airframe linear stability and control derivative models used in this analysis were generated with FlightCODE (Flight dynamics and control modeling tool for COnceptual DEsign), based on aircraft designs and performance maps obtained using the rotorcraft design tool NDARC (NASA Design and Analysis of Rotorcraft) (Ref. 7).

FlightCODE consists of an integrated collection of software tools previously referred to as “SIMPLI-FLYD” (SIMPLIfied FLIght dynamics for conceptual Design) and described in Ref. 8. FlightCODE enables a flight dynamics and control assessment of rotorcraft vehicle designs generated with NDARC. The approach uses a suite of tools including MATLAB/Simulink®, CONDUIT® and X-Plane® to generate flight dynamics models, analyze and optimize stability and control systems, and to enable real-time piloted simulation of the combined flight dynamic and control models.

A modular component-based approach, similar to that used in NDARC, is followed for modeling the linear, aerodynamics-dependent, stability and control derivative matrices. Calculations are performed for each rotor, wing, aerodynamic surface and fuselage component separately.

For calculation of the rotor contributions, the process uses numerical perturbation of a blade element model to calculate the stability and control derivatives. The blades are assumed rigid with a flapping hinge offset and spring to match the

modal flapping frequency. The rotor blade aerodynamics are quasi-steady, using table look-up or simple drag polar and linear curve slope approximation, of the blade section coefficients. Unsteady rotor wake effects are included by means of a 3-state dynamic inflow model by Peters-HaQuang, which accounts for wake curvature. The rotor model is initialized at the NDARC-calculated trim state and allowed to achieve steady state condition. For the other components, a simpler calculation of the linear derivatives is performed using a mix of analytical and empirical models.

Necessary adaptations in FlightCODE for this analysis included adding the option for modeling rotor shaft torque as a control input, redefining actuator model definitions to be compatible with multirotor collective-only configurations, and replacing the motors, previously modeled as simple second-order transfer functions, with an electric speed controller and motor model representative of the fundamental electro-mechanical parameters that may have relevance to handling qualities.

FlightCODE implements a model-following control law architecture (Figure 2) modeled in Simulink for the flight control system design. For analysis of the rotor speed-controlled configurations, the existing architecture was modified to include the multiple electric speed controllers and motors (Figure 3). From the block diagram it can be seen that the motor dynamics coupled, algebraically, with the bare-airframe through the drive system gear box, which related the rotor and motor speeds through gear box ratio r. In practice, the motor dynamics (propulsion system) were incorporated into the bare-airframe model itself, with the inputs then being defined by the motor voltages. This still left the rotor speed feedback loop, which implied that the actuator (motor and controller) were not fully decoupled from the bare-airframe dynamics as shown in Figure 2.

Linearized hover stability and control derivative bare-airframe models used for control system design and analysis retained only the four rotor speed (Ω_1, Ω_2, Ω_3 and Ω_4) degrees of freedom (in the case of the variable speed quadrotors), body translational (u, v and w) and angular (p, q and r) rate degrees of freedom, and Euler angle (ϕ, θ and ψ) rotations relative to the inertial frame, for 13 total retained states. Low-frequency (regressive) rotor flapping states, normally retained by FlightCODE were reduced out of the system to simplify the CONDUIT execution. This was verified to be acceptable. These modes were found to be highly damped (damping ratios greater than 0.9) despite their frequencies (6-8 rad/s) being in the range of flight control (0.1-10 rad/s), and therefore the phase drop was easily accounted for through an equivalent delay. Furthermore, control of these quadrotors was achieved primarily through thrust change, such that the coupling with the lateral or longitudinal rotor flapping modes would be minimized. This was confirmed through the comparison of the frequency responses of full and reduced order models.

Control system design optimization and analysis of the feedback and feedforward control gains was performed in CONDUIT by linking the model to handling qualities specifications. Specifications included constraints on stability and stability margins, disturbance rejection bandwidth and peak, crossover frequency, oscillatory behavior (eigenvalue damping), model following performance, actuator usage (root mean square, or RMS, metric) and rate-limiting (open-loop onset point, or OLOP, specification); and response-type

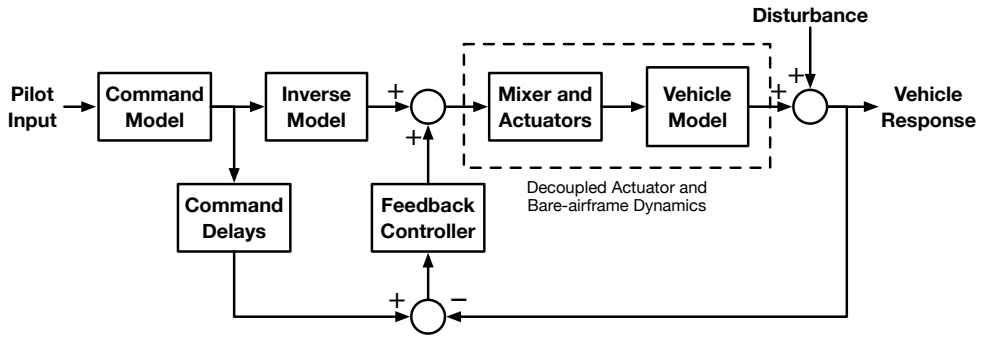

Figure 2. Model-following control system architecture

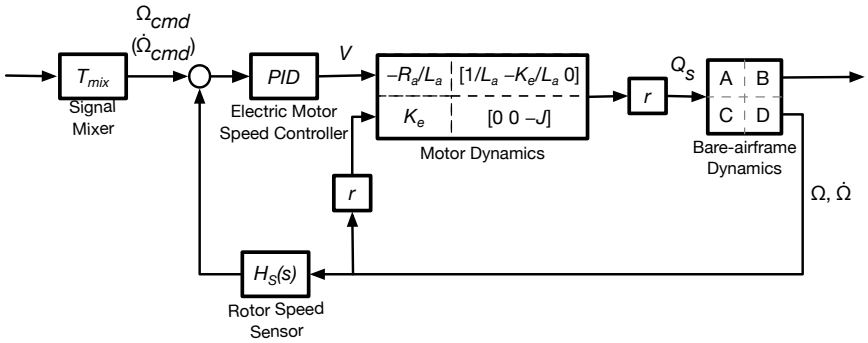

Figure 3. Block diagram of the electric motor and speed controller architecture

specifications such as short-term response, quickness and maximum attitude change specifications.

THEORY

Coupled Rotor-Motor Dynamics

The coupling of permanent magnet synchronous motors with flexible rotors has been explored before Ref. 9. The approach employed here simplifies some of the modeling assumptions but otherwise follows similar lines. The coupled motor-rotor mechanical equation of motion is given by

$$(I_r + Jr^2)\frac{d\Omega}{dt} = K_m r i_a + Q_A - Br^2\Omega \tag{1}$$

where I_r is the rotor inertia and J is the inertia of the high-speed drive components (motor and coupled transmission components), with drive system gear ratio r, such that the total angular momentum is $(I_r + Jr^2)$, K_m is the motor torque constant, i_a is the motor armature current, Q_A is the rotor aerodynamic torque and B is a linear representation of mechanical friction or viscous losses in the drive system.

The simplified motor armature electrical circuit equation is given by

$$L_a\frac{di_a}{dt} = -R_a i_a - K_e r\Omega + V_a \tag{2}$$

where L_a is the equivalent circuit armature inductance, R_a is the equivalent resistance, K_e is the back-EMF constant, and V_a is the voltage applied at the armature. Note that motor constant K_m is related to the back-EMF constant through the relationship $K_m = cK_e$, where proportionality constant c is the conversion factor between SI units (e.g., 0.7374 lb-ft/Nm).

Direct Drive Response Time Constant

Assuming $L_a = 0$, the fundamental dynamic response of the coupled motor-rotor direct drive system is given by

$$\frac{d\Omega}{dt} = \left[-\frac{cK_e^2 r^2}{R_a}\Omega + Q_A - Br^2\Omega + \frac{cK_e r}{R_a}V_a\right]\frac{1}{I_r + Jr^2} \tag{3}$$

Eq. 3, linearized, can be shown to have a single pole with natural time constant

$$T_c = -\frac{1}{\frac{\partial}{\partial\Omega}\left(\frac{d\Omega}{dt}\right)} \tag{4}$$

or

$$T_c = \frac{I_r + Jr^2}{\frac{cK_e^2 r^2}{R_a} - \frac{\partial Q_A}{\partial\Omega} + Br^2 - \frac{cK_e r}{R_a}\frac{\partial V_a}{\partial\Omega}} \tag{5}$$

These relationships provide some fundamental insight into the effect of the various parameters that govern the dynamic response of the rotor.

Clearly the time constant scales proportionally with the rotor and motor inertia, but the electrical properties of the motor and rotor aerodynamics need to be taken into account. The main contribution of the motor to the drive system pole is related to the back-EMF voltages generated in the circuit. Increased values of the K_e^2/R_a ratio can help reduce the rotor speed change response time. The role of the resistance in this situation would be seen as increasing the response time. The effect of proportional feedback in the speed controller can also be intuited from this relationship, as a negative $\partial V_a/\partial\Omega$ could be used to quicken the response. Finally, aerodynamic damping is seen to contribute to the reduction in the response time because the partial derivative $\partial Q_A/\partial\Omega$ is typically negative around nominal hover trim conditions. Naturally, the mechanical advantage of the gearbox between the motor and rotor needs to be selected to maximize the motor efficiency, given the nominal rotor design operating conditions, while minimizing the component weight. However, increased gearbox ratios can be seen to further help reduce the time constant. To obtain a sense of the significance of these parameters, however, it is necessary to ascertain their values.

Motor Parameter Characterization

Detailed or even specific motor data/models may typically not be available during the vehicle conceptual design stage. Moreover, the vehicle sizing task is concerned primarily with the motor steady state performance and component weight estimation. The procedure described here attempts to characterize motor dynamic and electrical parameters that are otherwise absent from the sizing solution using the assumption that only most basic information is available:

Back-EMF constant. Calculation of the motor back-EMF and related torque constants relies on the knowledge of the electric current drawn by the motor for a specific torque. The propulsion system engine size in NDARC is described by the sea level static power available per engine at specified takeoff rating, P_{eng}, and the specification propulsion group engine speed N_{spec}. Therefore, the relation

$$I = \frac{P_{eng}}{\eta V} \tag{6}$$

is employed with the assumption that the battery needs to supply a voltage, V, that is numerically approximately equal to the square root of P_{eng} (in watts). This assumption represents a compromise between high voltage systems which are penalized for the extra weight and volume required for insulation and high current systems which are penalized for the extra weight required for electrical switchgear and wiring. The battery sizing calculations in NDARC take into account the energy flow balance assuming a reference voltage V_{ref} = 4.2 V, which is typical of single lithium-ion battery cells. Thus, the voltage is formulated in terms of the number of cells connected in series to supply the required voltage,

$$V = N_s V_{ref} = \text{ceil}\left(\frac{\sqrt{P_{eng}}}{V_{ref}}\right)V_{ref} \tag{7}$$

The torque delivered by the motor at N_{spec} is P_{eng}/N_{spec}, such that the torque constant is given by

$$K_e = K_m = \frac{P_{eng}}{N_{spec} I} \tag{8}$$

It is noted that the numerical $K_e = K_m$ equivalency is valid only when quantities are given in SI units.

Motor resistance. Calculation of the motor resistance is based on an assumed motor efficiency; 95% efficiency is used for the rotor speed-controlled cases. It is noted that in steady state conditions

$$\frac{K_e^2}{R_a} = \frac{\eta}{1-\eta} \frac{P_{eng}}{\left(N_{spec}\right)^2} \tag{9}$$

such that

$$R_a = \frac{1-\eta}{\eta} \frac{\left(N_{spec}\right)^2}{P_{eng}} K_e^2 \tag{10}$$

Incidentally, it is observed that K_e^2/R_a, and consequently, the associated motor time constant is fundamentally related to the motor efficiency. Furthermore, the $\eta/(1-\eta)$ quotient presents a very steep slope in the vicinity of $\eta = 1$, suggesting the motor speed of response may be significantly impacted even by small reductions in the efficiency, which of course are related to the power losses through the equivalent circuit resistance.

Inertia. Estimation of the motor rotating inertia depends on assumptions about the geometry (length to diameter aspect ratio and rotor to stator weight fraction) of the motor, where

$$J = \frac{1}{2} M \left(\frac{D_e}{2}\right)^2 f_d \tag{11}$$

is the moment of inertia of a cylinder of mass M and external diameter D_e. Inertia factor f_d accounts in a simple way for high speed drive system components coupled to the motor. The weight of the motors is calculated in the sizing analysis and is a function of the peak torque. Motor density is typically 100–250 lb/ft^3 but values exhibit significant variation (Ref. 7). An average value of 175 lb/ft^3 was chosen for this study.

Inductance. Axial flux motors present an alternative architecture gaining popularity for aviation applications because of their more compact nature and improved power-to-weight ratios (Refs. 10–14). An axial flux motor places the permanent magnets on the face of the rotor and puts the stator in front of the rotor. The following figure shows equivalent inductance values estimated from d- and q-axis inductances for three different axial flux motors and voltage-current combinations (Ref. 15).

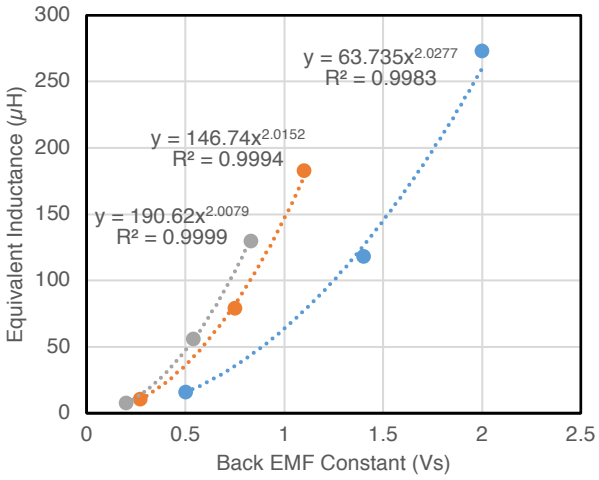

Figure 4. Inductance relationships as a function of back motor EMF constant

The three motors approximately follow the quadratic trend described by,

$$L_a = \lambda(\tau) K_e^2 \tag{12}$$

where $\lambda(\tau)$ is a proportionality constant, which is a function of the torque or power rating. A linear least square fit based on these three data points yields the following approximation:

$$\lambda(\tau) = 244.22 - 0.7287\tau \tag{13}$$

as a function of the continuous torque rating. Note that, based on these state-of-the-art motors, expected inductance values are on the order of a few microhenry and result in extremely low time constants of the current dynamics. Therefore, the assumption was made that the electric current response was instantaneous.

RESULTS

Vehicle Sizing

General characteristics of all eight quadrotor configurations sized in NDARC are shown in Table 1. Figure 5 shows the design gross weight as a function of passenger capacity. As design gross weight increases, results suggest the difference in weight between the collective- and rotor speed-controlled variants increases non-insignificantly, with the difference for the 6-passenger variants reaching 762.5 lb. Trends shown in Figures 6–8 for both configurations reveal that moments of inertia of rotor and motor components scale uniquely as a function of design gross weight. However, it should be noted that these calculations do not include the contribution of the cross shafts and other drive system components of the collective-controlled variants. Figures 9 and 10 show the motor back-EMF-related torque quotients. These quotients clearly scale directly in proportion to P_{eng} because motor reference speed N_{spec} and efficiency values were assumed constant for all design points in the sizing analysis.

Table 1. General design characteristics of quadrotor configurations

Parameter (units)	Collective Control				Rotor Speed Control			
	1-Pax	2-Pax	4-Pax	6-Pax	1-Pax	2-Pax	4-Pax	6-Pax
Design Gross Weight (lb)	1324.81	2752.71	4713.46	6479.94	1287.17	2292.36	4163.74	5716.42
- Payload	250.00	400.00	800.00	1200.00	250.00	400.00	800.00	1200.00
- Weight Empty	1069.71	2343.02	3902.33	5269.20	1031.83	1882.09	3353.44	4506.67
- Operating Weight	1074.71	2353.02	3912.33	5279.20	1036.83	1892.09	3363.44	4516.67
Number of Rotors	4	4	4	4	4	4	4	4
Disk Loading (lb/ft^2)	2.5	3.0	3.0	3.0	2.5	3.0	3.0	3.0
Number of Blades	3	3	3	3	3	3	3	3
Rotor Radius (ft)	6.5	8.5	11.2	13.1	6.4	7.8	10.5	12.3
Solidity, thrust-weighted	0.065	0.055	0.055	0.055	0.065	0.055	0.055	0.055
Hover Tip-Speed (ft/s)	450.0	550.0	550.0	550.0	450.0	550.0	550.0	550.0
Rotational Speed (rad/s)	69.3	64.4	49.2	42.0	70.3	70.5	52.3	44.7
Flapping Frequency (/rev)	1.030	1.030	1.030	1.030	1.030	1.030	1.030	1.030
Lock Number	3.69	3.88	4.64	5.16	3.66	3.65	4.45	4.95
Rotor Design Thrust (lb)	346.6	941.2	1597.8	2174.7	338.2	662.4	1204.1	1643.0
Rotor Design Power (hp)	21.3	70.4	119.2	161.5	20.8	46.2	83.9	114.2
Moments of Inertia (slug ft^2)								
- I_{xx}	779.47	2804.36	8222.3	15540.1	735.81	1944.81	6416.22	12093.7
- I_{yy}	850.83	3061.12	8975.1	16963.0	803.18	2122.87	7003.67	13201.0
- I_{zz}	1029.51	3703.96	10859.9	20525.2	971.85	2568.67	8474.44	15973.2
- I_{xy}	0	0	0	0	0	0	0	0
- I_{yz}	0	0	0	0	0	0	0	0
- I_{xz}	0	0	0	0	0	0	0	0
Rotor Inertia (slug ft^2)	12.8927	41.6001	133.397	265.841	12.1123	27.9836	101.968	202.611
Specification Engine Speed, all engines (rpm)	8000	8000	8000	8000	8000	8000	8000	8000
SLS Power Available (hp)								
- Engine Group 1	22.8	71.0	122.4	168.0	23.5	51.5	96.4	130.5
- Engine Group 2	22.8	71.0	122.4	168.0	23.5	51.5	96.5	130.5
- Engine Group 3	22.8	71.0	122.4	168.0	23.5	63.5	120.8	165.1
- Engine Group 4	22.8	71.0	122.4	168.0	23.5	63.5	120.8	165.1
Battery Capacity (MJ)	186.5	574.5	977.4	1330.9	176.0	470.1	886.1	1196.4

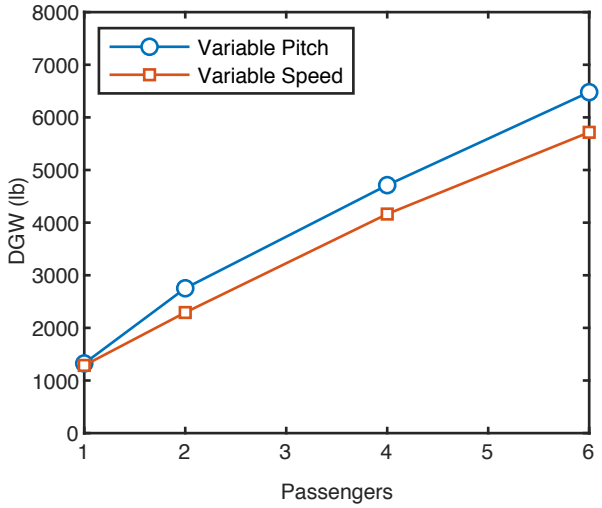

Figure 5. Design gross weight for all vehicle configurations

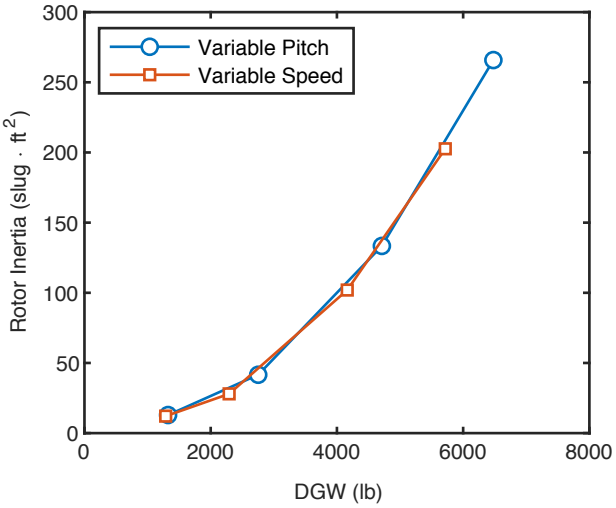

Figure 6. Rotor inertia for vehicle design gross weight

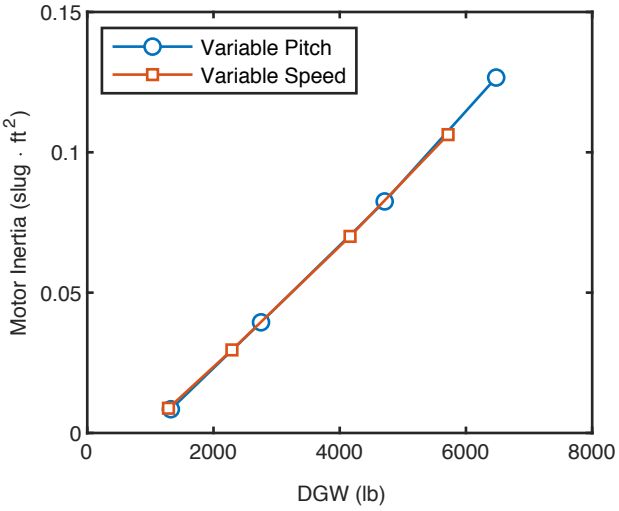

Figure 7. Motor inertia for vehicle design gross weight

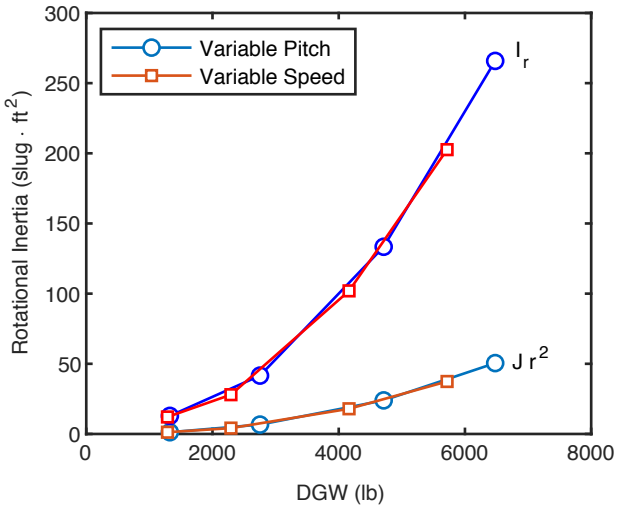

Figure 8. Effective rotational inertia of rotor and motor components

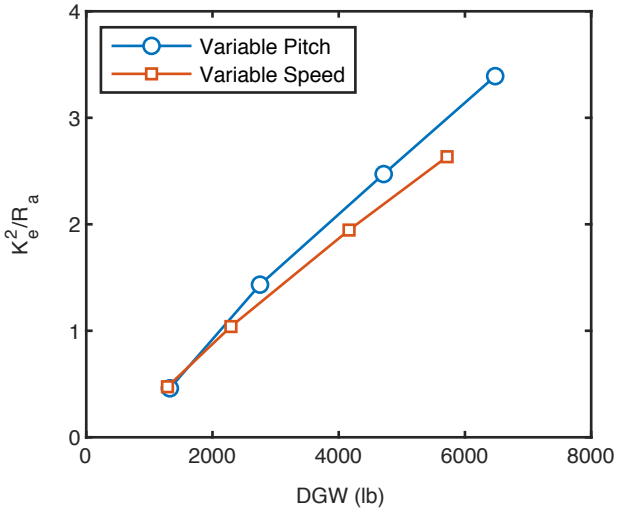

Figure 9. Effect of design gross weight on back-EMF motor torque quotient

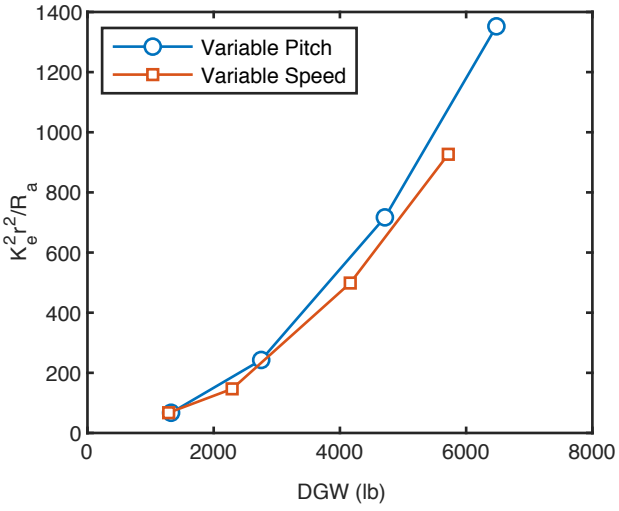

Figure 10. Effect of design gross weight on back-EMF shaft torque quotient

The significance of these trends is understood when comparing the effect on the rotor response eigenvalues (Figure 11) and the associated time constant (Figure 12) for the variable speed configurations. As the design gross weight increases the natural response of the rotor varies from about 0.24 s (for the single-passenger quadrotor) to approximately 0.32 s (for the 6-passenger variant). From a handling qualities perspective, nearly 80 ms is not an insignificant increase in the open-loop or bare-airframe dynamics. This increase is over an already onerous 240 ms time constant for the single-passenger variant. The full analysis needs to consider also the motor speed controller, and of course vehicle dynamics. Loss of control effectiveness can potentially be intuited from Eq. 3, where the ratio of the control to stability derivatives can be found to be inversely proportional to the shaft torque constant $K_e r$ (Figure 13). Accordingly, voltage control inputs would have to be three to four times larger to induce the same steady state rotor response in the 6-passenger quadrotor as in the single-passenger variant.

Motor Speed Controller

Motor speed controllers were configured as PI or PID regulators, one for each rotor drive. All four controllers were identical, however, such that the solution method only needed to solve for two (in case of PI controller) or three (for PID) gains. The optimization approach was based on the linearized model, with all rigid body states fixed. The gains were selected to simultaneously minimize the rotor speed response rise time (measured from 10% to 90% of the peak) and motor current RMS. Without the latter constraint, the solution method would ignore the limitations of the motors as noted in Ref. 3. Alternatively, closed-loop bandwidth or impulse response settling times could be employed to the same effect, instead of the rise time objective constraint.

Some system limits may not be known during conceptual design. Rotor speed may be limited by structural modes or operational constraints, such as acoustics. In absence of clearly defined rotor speed limits, 12% margins over the

hover trim value were assumed to define the maximum rotor speed. These translated to ±8.5, ±8, ±6 and ±5 rad/s for the 1-, 2-, 4- and 6-passenger configurations, respectively. Mechanical torque limits (translated into motor current) as a function of P_{eng} are shown in Figure 14 alongside the motor current required for hover trim flight of the four different sized quadrotors. The difference between the limits and the trim value defines the allowable margins for the control optimization solution. Battery discharge current limits are given in terms of the maximum burst discharge rate, x_{mbd}. Even with the assumption that all four motors would concurrently demand power from the batteries at a discharge rate of x_{mbd}, the electrical current limits for each motor are an order of magnitude higher than the mechanical limits, based on the battery charge capacity predicted from the sizing analysis. Drive system torque limits evidently were the most constraining, allowing only for 10, 24, 44 and 50 A maximum motor current changes from the trim analysis point.

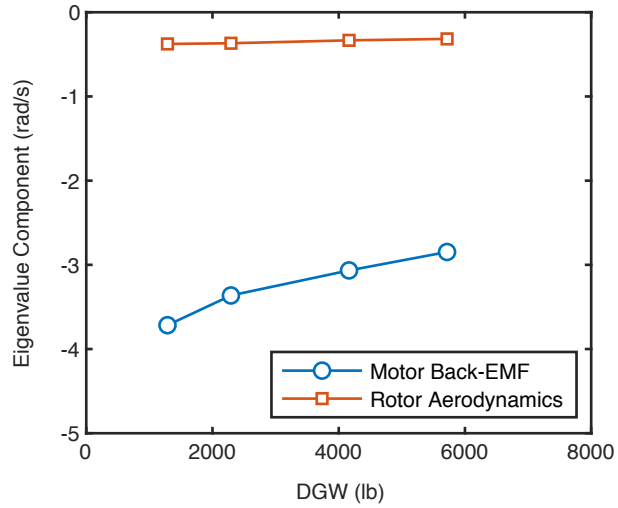

Figure 11. Effect of design gross weight on rotor response eigenvalues

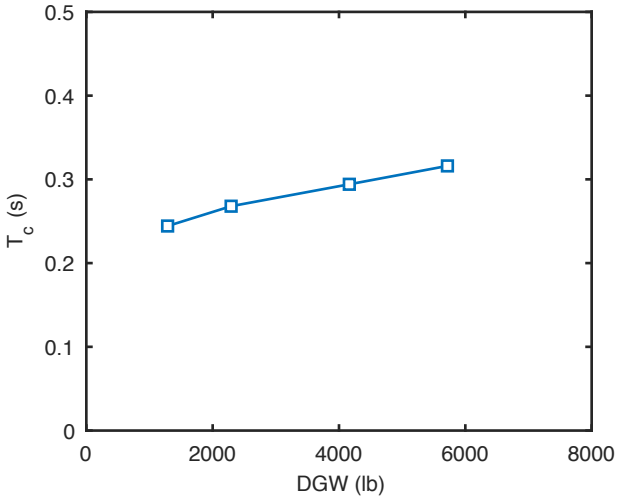

Figure 12. Effect of design gross weight on rotor response time constant

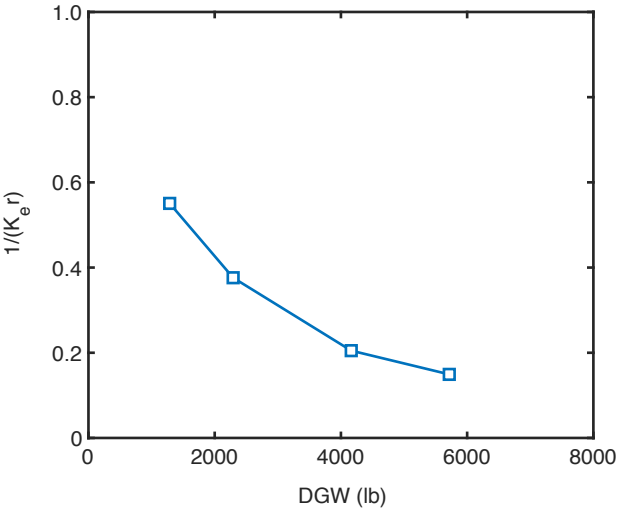

Figure 13. Effect of design gross weight on motor control power

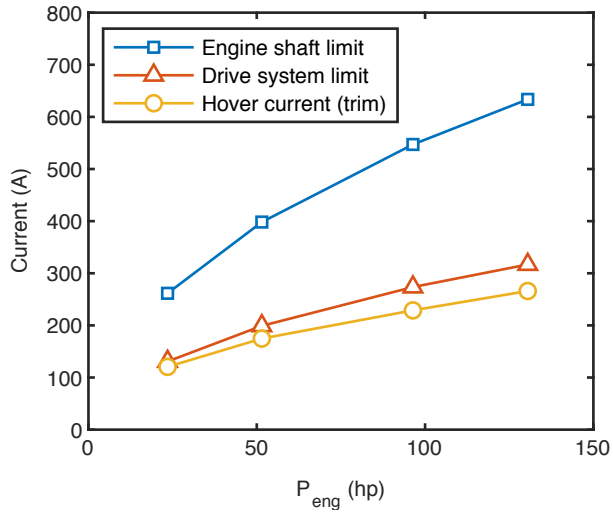

Figure 14. Electrical equivalent of mechanical torque limits

Optimization of the speed controller was performed in CONDUIT considering the "good" and "bad" limits in Table 2. The stability margin and low-frequency response requirements were the only hard constraints the optimization algorithm was required to satisfy.

Table 2. Speed controller optimization parameter limits

Parameter	Units	"Good"	"Bad"
Gain Margin	dB	7	6
Phase Margin	deg	60	45
Damping Ratio	–	0.9	0.8
Low-Frequency Magnitude[a]	dB	0.5	3.0

[a] 0.01–0.5 rad/s range

Weighing the proposed drive system limits in the control system optimization process resulted in nearly identical rotor speed response rise times (~1 s) of all four aircraft (Table 3). Accordingly, actuator usage, as quantified by the weighted

RMS of the motor electrical current output, was also approximately similar (~1.5–1.6) for all four configurations (Table 2).

Table 3. Speed controller optimization results

Parameter	Units	1-Pax	2-Pax	4-Pax	6-Pax
Rise Time	s	1.1297	1.0146	0.9832	1.0
RMS	–	1.5649	1.5073	1.4921	1.6086

Interestingly, while the rotors for the single-passenger configuration were the smallest and lightest, the speed controller for this configuration had the worst performance characteristics. The limits imposed on the controller optimization, as informed by the conceptual design, were in fact the most stringent. Therefore, the controller prohibited the motor from accelerating the rotor any more quickly than the larger rotors from the 2-, 4- or even the 6-passenger configurations.

This result led to further investigation into the effect of motor drive limits on the performance of the speed controller. Figure 15 shows the resulting rise time specification of the single-passenger rotor, for three different gain iterations: 1) nominal gains for 1-passenger configuration, 2) gains computed by enforcing the same limits as for the 6-passenger configuration (±5 rad/s maximum rotor speed change and maximum current change of 50 A); and 3) gains for a maximum ±200 A motor current limit. The rotor speed step responses for these three gain sets are shown in Figure 16. The current is seen in Figure 17 to peak up to almost 200 A, instantaneously, after the step is applied and then settle down within 1.13 s. Equivalently, the problem could be analyzed from the optic of the effect of reducing the rotor inertia. Fundamentally, the question is whether the control system has the required control power to inertia ratio.

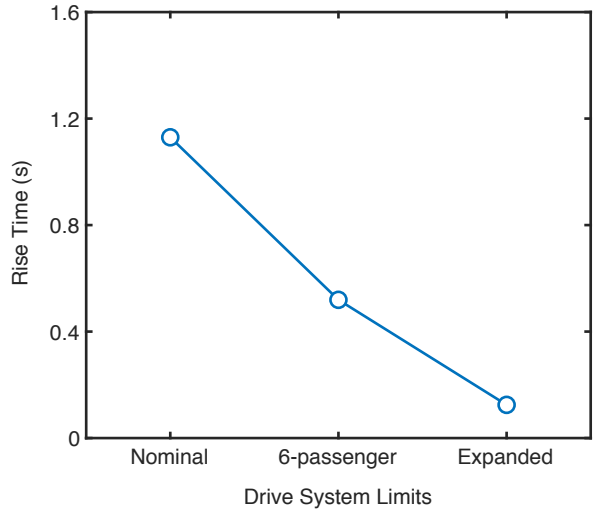

Figure 15. Effect of maximum allowed speed change and motor current on speed controller optimization

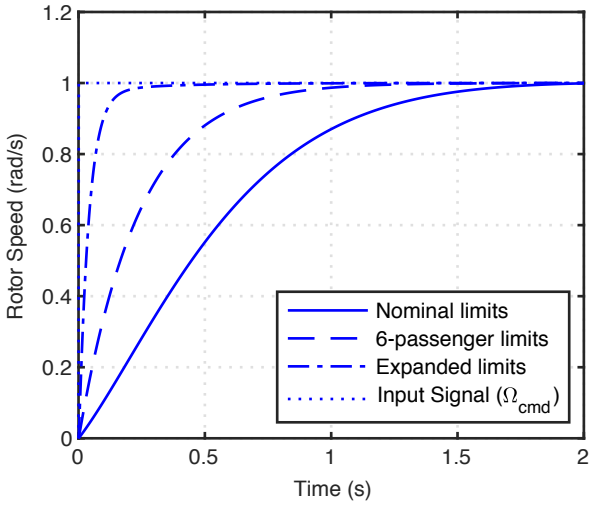

Figure 16. Rotor speed step response for different speed change and motor current limits (1-passenger quadrotor)

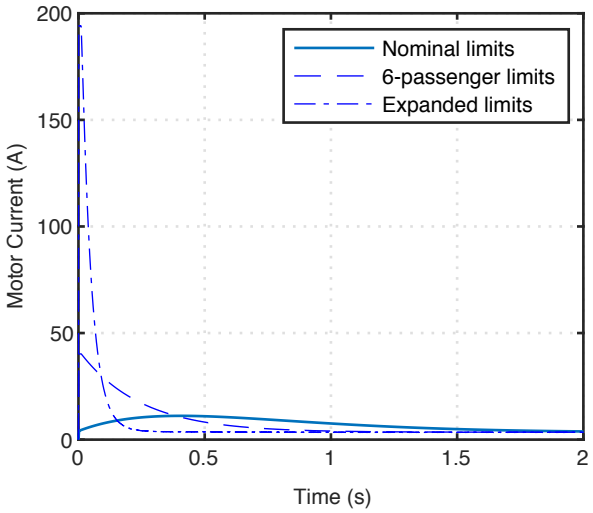

Figure 17. Motor current step response for different speed change and motor current limits (1-passenger quadrotor)

Collective Control

Results for control system stability margins, disturbance rejection bandwidth, crossover frequency, actuator rate-limiting and usage; and response-type specification values can be found in Table 4 for heave, Table 5 for roll, and Table 6 for yaw. For the feedback gain optimization, actuator open-loop onset-point and RMS values were driven by an attitude or vertical velocity disturbance, such as would be induced by wind gusts or turbulence, while for the command model optimization they were driven by pilot input. As indicated in the maximum deviation column of the tables, the control and handling qualities specifications did not vary significantly as the size of the vehicle increased. The heave, roll, and yaw cases were able to converge to phase 3 during the CONDUIT optimization, meaning all specifications converged to Level 1 or "good" handling qualities. This implies that all four sizes of collective controlled quadrotor are feasible from a controllability perspective.

Table 4. Heave control optimization results for collective-controlled quadrotors

Parameter	Unit	1-Pax	2-Pax	4-Pax	6-Pax	Average	Maximum Deviation
Stability Gain Margin	dB	24.8	24.5	24.5	24.4	24.5	0.3
Stability Phase Margin	deg	99.9	96.6	95.8	95.8	97.0	4.2
Disturbance Rejection Bandwidth	rad/s	1.0	1.0	1.0	1.0	1.0	0.0
OLOP Phase (disturbance)	deg	-140.0	-140.0	-140.0	-140.0	-140.0	0.0
OLOP Amplitude (disturbance)	dB	-15.0	-15.0	-15.0	-15.0	-15.0	0.0
Crossover Frequency	rad/s	0.86	0.91	0.92	0.92	0.90	0.05
Actuator RMS (disturbance)	–	0.02	0.02	0.02	0.02	0.02	0.00
Vertical Climb Rate	ft/min	223.0	223.0	223.0	223.0	223.0	0.0
OLOP Phase (pilot input)	deg	-305.9	-140.0	-140.0	-140.0	-181.5	165.9
OLOP Amplitude (pilot input)	dB	-37.6	-15.0	-15.0	-15.0	-20.7	22.6
Actuator RMS (pilot input)	–	0.02	0.02	0.02	0.02	0.02	0.00

Table 5. Roll control optimization results for collective-controlled quadrotors

Parameter	Unit	1-Pax	2-Pax	4-Pax	6-Pax	Average	Maximum Deviation
Stability Gain Margin	dB	13.5	13.7	13.8	13.9	13.7	0.4
Stability Phase Margin	deg	59.4	55.4	53.4	52.3	55.1	7.1
Disturbance Rejection Bandwidth	rad/s	1.2	1.2	1.2	1.2	1.2	0.0
OLOP Phase (disturbance)	deg	-140.0	-140.0	-195.0	-172.9	-162.0	55.0
OLOP Amplitude (disturbance)	dB	-15.0	-15.0	-15.4	-13.1	-14.6	2.3
Crossover Frequency	rad/s	3.3	3.3	3.3	3.3	3.3	0.0
Actuator RMS (disturbance)	–	0.02	0.02	0.03	0.04	0.03	0.01
Bandwidth	rad/s	5.1	4.9	4.9	6.0	5.2	1.2
Phase Delay	s	0.03	0.03	0.03	0.03	0.03	0.00
Achievable Yaw Rate	deg/s	200.1	207.7	194.1	136.3	184.6	71.4
Minimum Attitude Change (1)	deg	15.5	16.5	16.6	13.7	15.6	2.9
Peak Rate to Attitude Ratio (1)	1/s	1.65	1.62	1.61	1.70	1.65	
Minimum Attitude Change (2)	deg	41.3	44.0	44.3	31.9	40.4	12.4
Peak Rate to Attitude Ratio (2)	1/s	1.01	1.00	1.00	1.14	1.04	
Minimum Attitude Change (3)	deg	69.7	66.0	66.5	54.7	64.2	15.0
Peak Rate to Attitude Ratio (3)	1/s	0.90	1.00	1.00	1.00	0.97	
OLOP Phase (pilot input)	deg	-124.5	-126.4	-126.9	-128.0	-126.5	3.5
OLOP Amplitude (pilot input)	dB	-3.42	-2.54	-1.10	-1.20	-2.06	2.32
Actuator RMS (pilot input)	–	0.18	0.22	0.28	0.35	0.26	0.16

Table 6. Yaw control optimization results for collective-controlled quadrotors

Parameter	Unit	1-Pax	2-Pax	4-Pax	6-Pax	Average	Maximum Deviation
Stability Gain Margin	dB	10.1	10.5	11.0	11.6	10.8	1.4
Stability Phase Margin	deg	48.3	48.6	50.3	51.5	49.7	3.1
Disturbance Rejection Bandwidth	rad/s	0.91	0.89	0.82	0.79	0.85	0.12
OLOP Phase (disturbance)	deg	-131.1	-130.7	-129.3	-128.4	-129.9	2.7
OLOP Amplitude (disturbance)	dB	0.58	1.59	1.83	1.74	1.44	1.25
Crossover Frequency	rad/s	4.6	4.4	4.1	3.9	4.2	0.7
Actuator RMS (disturbance)	–	0.13	0.16	0.18	0.19	0.16	0.06
Bandwidth	rad/s	1.3	1.1	0.9	0.8	1.0	0.4
Phase Delay	s	0.03	0.03	0.03	0.03	0.03	0.00
Achievable Yaw Rate	deg/s	30.2	30.0	30.0	30.0	30.0	0.2
Minimum Attitude Change (1)	deg	15.1	15.0	15.0	15.0	15.0	0.2
Peak Rate to Attitude Ratio (1)	1/s	0.83	0.77	0.67	0.63	0.73	0.21
Minimum Attitude Change (2)	deg	34.1	33.9	33.7	33.5	33.8	0.6
Peak Rate to Attitude Ratio (2)	1/s	0.51	0.49	0.46	0.44	0.48	0.07
Minimum Attitude Change (3)	deg	72.2	71.6	71.0	70.4	71.3	1.8
Peak Rate to Attitude Ratio (3)	1/s	0.40	0.39	0.37	0.36	0.38	0.03
OLOP Phase (pilot input)	deg	-131.0	-130.8	-129.3	-128.4	-129.9	2.6
OLOP Amplitude (pilot input)	dB	0.71	1.84	1.89	1.75	1.55	1.18
Actuator RMS (pilot input)	–	0.15	0.18	0.19	0.20	0.18	0.05

For the collective controlled vehicles, rotor speed was held constant and a motor speed controller was not employed. Although these additions would most likely not significantly affect the magnitude of the specifications, it is hypothesized from the results of the rotor speed controller study that the addition of motor dynamics could produce some deviation between vehicle sizes than is currently seen for the yaw case. Incorporating these additions to the model is planned as part of near-term future work. Additionally, it should be noted that these results do not incorporate any consideration for drive system torque or any other physical limits. Therefore, it should also be further investigated in the future if torque limits affect the feasibility of the designs.

Figures 18, 19, 20, 21 and 22 contain the specifications that varied as the number of passengers increased. Yaw control bandwidth was found to be lowest (0.8 rad/s) and a propensity for rate-limiting triggered PIO in yaw was identified. Yaw appeared to be relatively consistent over the vehicle size trade space compared to roll, but this is most likely due to the modeling simplification described above. It is hypothesized that yaw trends would more closely match the roll trends in Figures 17–20 if the electric components were accounted for more comprehensively. Because of this, focus will be placed on roll for discussion.

An inverse relationship exists in the roll case between quickness and maximum roll rate values (Figures 18–20) and bandwidth (Figure 20). Quickness and maximum roll rate decrease as number of passengers increases, while attitude bandwidth increases with increased number of passengers between the four and six passenger configurations. An increase also occurs in actuator usage between four and six passengers (Figure 21). One possible explanation is that in order to minimize actuator usage, the quickness, and related roll rate, must decrease. This trade-off warrants further investigation.

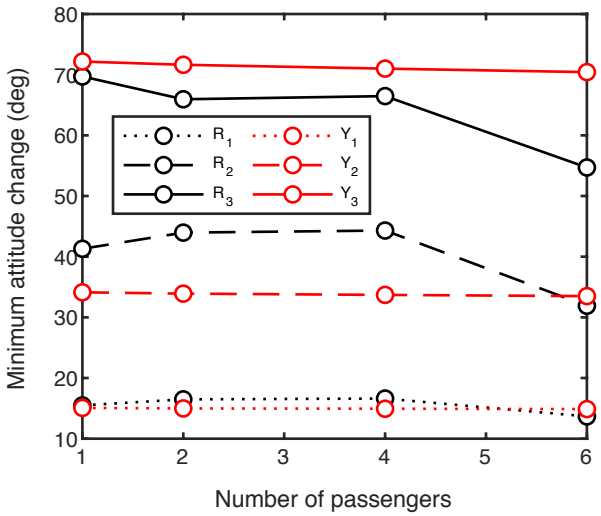

Figure 18. Minimum attitude and heading changes versus size (passenger capacity): roll (R_i) and yaw (Y_i)

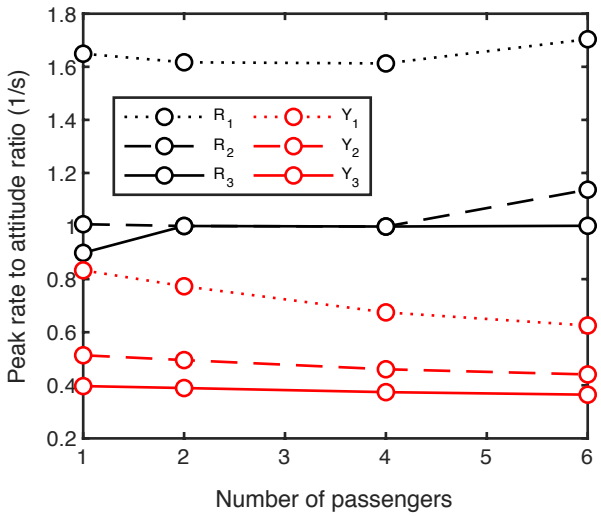

Figure 19. Peak rate to angular change quickness specification versus size (passenger capacity): roll (R_i) and yaw (Y_i)

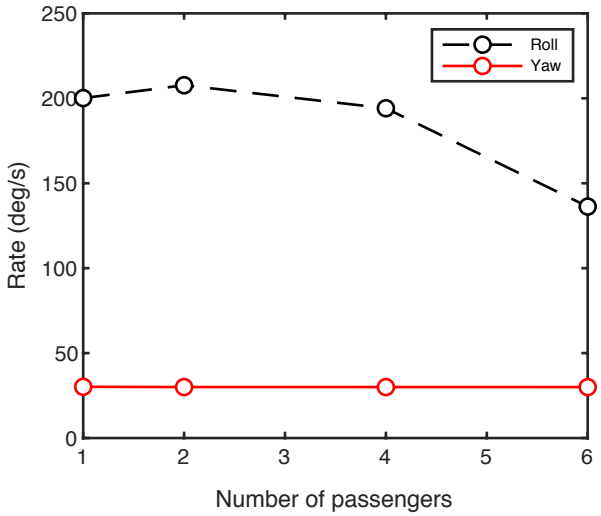

Figure 20. Achievable angular rate versus size (passenger capacity)

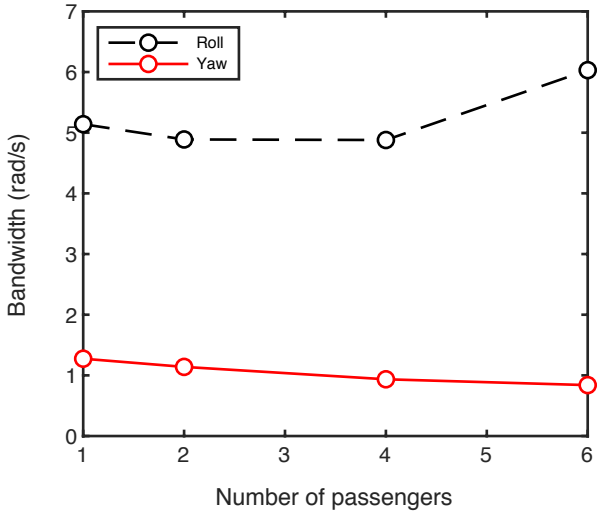

Figure 21. Attitude and heading response bandwidth versus size (passenger capacity)

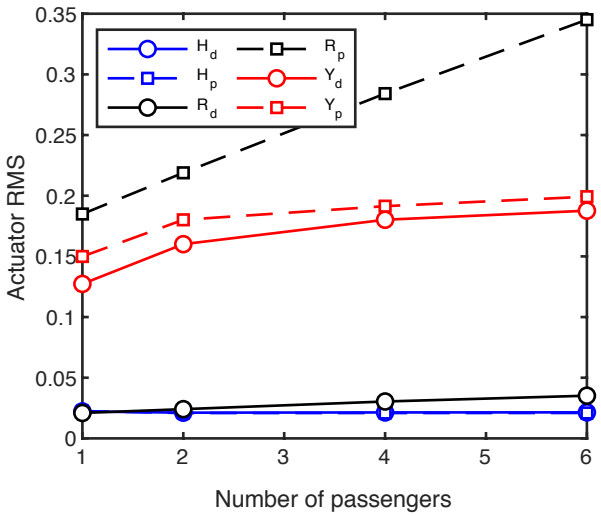

Figure 22. Actuator usage versus size (passenger capacity) for disturbance (d subscript) and pilot (p subscript) inputs: heave (H_d and H_p), roll (R_d and R_p) and yaw (Y_d and Y_p)

Rotor Speed Control

As is normal of all rotorcraft, the four different quadrotor designs considered here are open-loop unstable in roll and pitch. The first step in ascertaining effectiveness of using variable rotor speed for control of the vehicle is to determine whether it is possible to stabilize the vehicle. Figures 23 and 24 illustrate the challenge in doing so. Figure 23 shows the effect on rate stabilization, while Figure 24 considers attitude stabilization feedback only. The broken-loop frequency responses shown in Figures 23 and 24 account for ESC, motor, bare-airframe and all sensor dynamics and delays. Although the crossover frequencies and stability margins are not shown on the figures, it would be easy to see that stability margins in both instances were negative. Incidentally, the pitch axis broken-loop responses (not shown) exhibited very similar behavior, which was unsurprising considering the near symmetry of lateral and longitudinal dynamics of these quadrotors in hover. It was therefore not possible to stabilize the roll (and pitch) axis with a crossover frequency that provided adequate disturbance rejection and model-following performance.

The second aspect of significance discernible from Figures 23 and 24 is how little difference there was in the broken-loop responses for the four different configurations. As with the rotor speed controllers, and perhaps consequentially, the stability margins for the single-passenger configuration were found to be slightly worse than those of the larger aircraft. The effect of rotor speed controller bandwidth on the overall broken-loop roll response is shown in Figure 25. Firstly, it can be imagined that only a slight reduction in the rotor speed controller rise time (such that T_r = 1 s) could perhaps force the broken-loop response to match the 2-, 4- and 6-passenger broken-loop responses in Figures 23 and 24 better. Secondly, while the stability margins are shown to improve slightly, the change in rotor speed controller rise time was still insufficient to reverse the closed-loop instability.

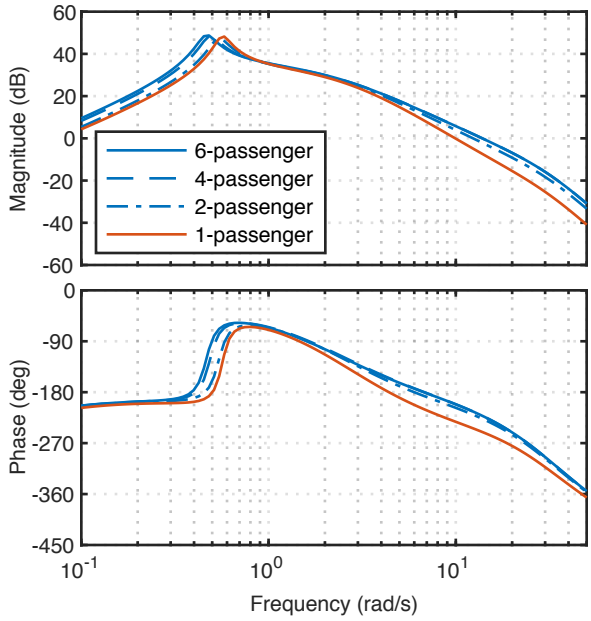

Figure 23. Broken-loop roll response with unity rate feedback (K_p = 1.0) for all four quadrotor configurations

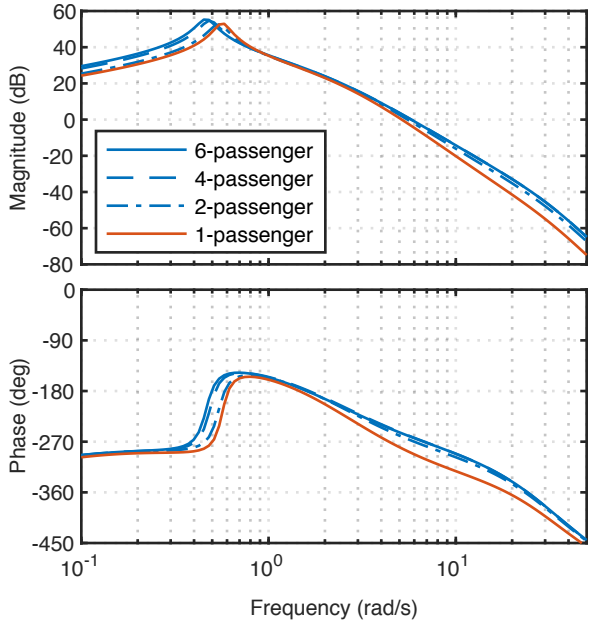

Figure 24. Broken-loop roll response with unity proportional feedback (K_ϕ = 1.0) for all four quadrotor configurations

The fundamental characteristics of the broken-loop responses are shown to be inherited primarily from the coupled motor and bare-airframe dynamics, shown in Figures 26 and 27 in response to a roll-aligned voltage command into the four motors of the 1-passenger configuration. Stability margins for rate feedback stabilization are seen in Figure 26 to improve significantly in the absence of sensor and other sources of delay. Attitude feedback stability margins from the bare-airframe are clearly negative initially. Added delay degrades the margins even further. Relating back to the vehicle design, it is shown in Figure 27 that increasing the control power to inertia ratio by scaling down the inertia by one full order of magnitude is enough to significantly improve the stability margins. The drawback of reducing the vehicle roll inertia was the emergence of a sharp resonance peak at the phugoid frequency. Although not analyzed in any detail here, these types of phenomena often present feedback sensitivity issues.

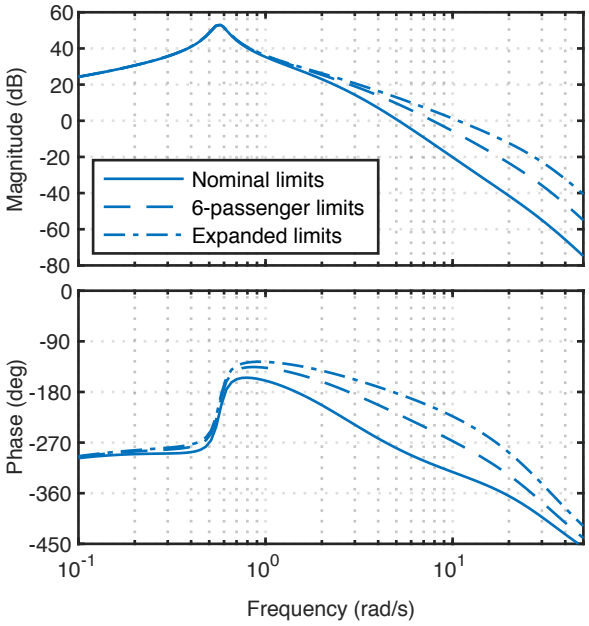

Figure 25. Broken-loop roll response with unity proportional feedback (K_ϕ = 1.0) for 1-passenger quadrotor with ESC optimized to different limits

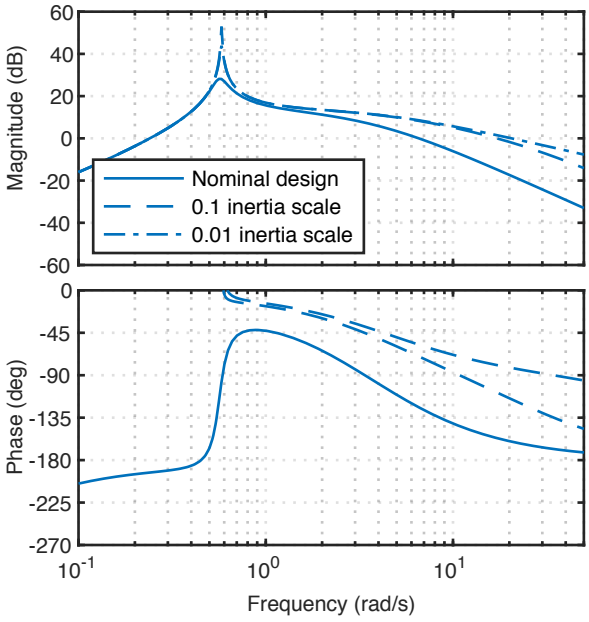

Figure 26. Effect of inertia on bare-airframe roll rate response to lateral motor voltage input for 1-passenger quadrotor

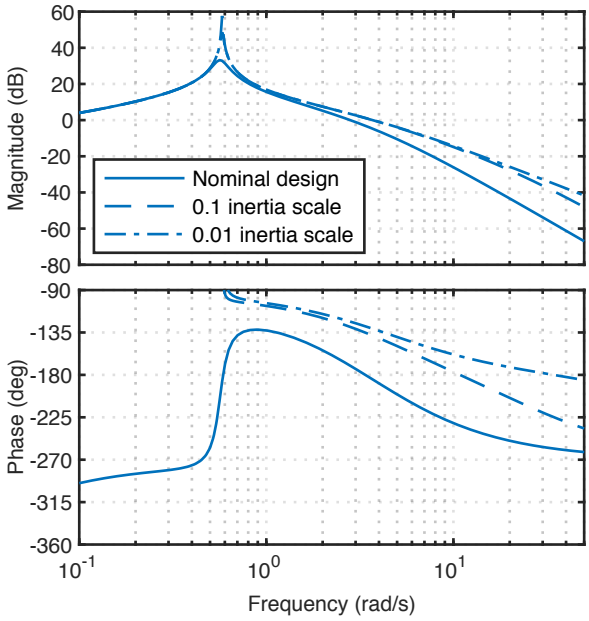

Figure 27. Effect of inertia on bare-airframe roll attitude response to lateral motor voltage input for 1-passenger quadrotor

SUMMARY OF RESULTS AND DISCUSSION

The design of flight control systems for eight electric propulsion quadrotor configurations of varying gross weight, four using variable rotor speed and four using variable collective blade pitch for control, was informed by conceptual design parameters. Effects of vehicle and rotor inertias, motor electric and mechanical parameters, battery discharge characteristics, and various propulsion system limits on the control system performance and handling qualities metrics were explored to varying levels of detail, in particular for configurations using variable rotor speed for control.

Generally, handling qualities metrics were found to vary little despite relatively large variation in the specific vehicle design parameters. This was because competing parameters tended to scale proportionally. For example, whereas rotor inertia increased approximately quadratically with respect to vehicle design gross weight, the motor torque constants and drive system limits scaled proportionally. Consequently, the motor speed controllers resulted in very similar performance characteristics. Similar arguments could be extended to the relationship between vehicle inertia and control power obtained from the rotors (rotor thrust and torque). This exploratory work has led to the hypothesis that control power to inertia ratio remains relatively constant, based on the current vehicle sizing rules.

Finally, results suggested there is a significant difference in controllability between the blade pitch- (collective-) and rotor speed-controlled variants, with the variants using collective easily meeting the Level 1 handling qualities and control system specifications. This result is compared to the rotor speed-controlled variants which showed negative stability margins in the open-loop roll (and pitch) transfer functions, indicating the closed-loop will be unstable. This represents a problem for open-loop unstable systems, as most rotorcraft are, because it is not possible to increase the feedback gains in order to stabilize the aircraft dynamics. Stable solutions were obtained by reducing the feedback gains, but these did not meet minimum performance requirements. Reductions in the vehicle inertia, coupled with faster rotor speed controller response times could perhaps be sufficient to reverse the negative margins of the system. Further exploration of these possibilities was, however, beyond the scope of the current study. Although performed for different scales of vehicle, the results from Ivler et al. (Ref. [16]) were consistent with the trends observed here.

CONCLUSION

The following conclusions are established, based on the results and discussion presented in this study:

- Conceptual design information, such as that originating from NDARC, was sufficient to inform the design of flight control systems for various concept quadrotor designs with electric propulsion, but models perhaps need to be revisited to ascertain their validity and adequacy.
- In general terms, control power to inertia remained invariant as a function of design gross weight, and therefore vehicle size did not seem to change the handling qualities specifications much.
- In the absence of motor dynamics, collective-controlled quadrotor configurations were feasible and met Level 1 handling qualities specifications.
- Variable rotor speed-controlled quadrotors sized for UAM were not stabilizable with adequate closed-loop performance, based on the current drive system mechanical limits and technology factors (inertias) programmed into the sizing analysis.

FUTURE WORK

Based on the findings of this study, the following areas of future emphasis have been identified:

1. Refine the rotor aeromechanics models to include dynamics inflow and rotor coning dynamics.
2. Validate and refine the conceptual design sizing models or assumption of the various design parameters that inform the flight control design, in particular the motor electrical and mechanical properties.
3. Investigate effects of technology factors on these parameters and flight control system design performance and handling qualities metrics.
4. Evaluate configurations in piloted simulation.

ACKNOWLEDGEMENTS

The authors would like to thank and acknowledge fellow NASA Ames Research Center Aeromechanics Branch members, Wayne Johnson, Chris Silva, and Lee Kohlman.

Johnson and Silva are responsible for the RVLT concept vehicles and NDARC designs. Kohlman contributed to this work through his knowledge of power systems. The authors would also like to thank Ames Intelligent Systems Division contributors, Stefan Schuet, John Kaneshige, and Thomas Lombaerts for their valuable perspective and feedback.

REFERENCES

[1] Johnson, W., Silva, C., and Solis, E., "Concept Vehicles for VTOL Air Taxi Operations," Presented at the American Helicopter Society Technical Conference on Aeromechanics Design for Transformative Vertical Flight, San Francisco, CA, January 16–19, 2018.

[2] Silva, C., Johnson, W., Antcliff, K. R., and Patterson, M. D., "VTOL Urban Air Mobility Concept Vehicles for Technology Development," Paper AIAA 2018-3847, 2018 Aviation Technology, Integration, and Operations Conference, AIAA AVIATION Forum, Atlanta, GA, June 25–29, 2018.

[3] Walter, A., McKay, M., Niemiec, R., Gandhi, F. and Ivler, C., "Handling Qualities Based Assessment of Scalability for Variable-RPM Electric Multi-Rotor Aircraft," Proceedings of the 75th Vertical Flight Society Annual Forum, Philadelphia, Pennsylvania, May 13-16, 2019.

[4] U. Saetti, J. F. Horn, S. Lakhmani, C. Lagoa, and T. Berger, "Design of Dynamic Inversion and Explicit Model Following Control Laws for Quadrotor Inner and Outer Loops," Annual Forum Proceedings - American Helicopter Society International, Vol. 2018-May, 2018.

[5] Ivler, C. M. , Rowe, E. S., Martin, J., Lopez, M. J. S., and Tischler, M. B., "System Identification Guidance for Multirotor Aircraft: Dynamic Scaling and Test Techniques," Proceedings of the 75th Vertical Flight Society Annual Forum, Philadelphia, Pennsylvania, May 13-16, 2019.

[6] Lombaerts, T., Kaneshige, J., Schuet, S., Hardy, G., Aponso, B., and Shish, K., "Nonlinear Dynamic Inversion Based Attitude Control for a Hovering Quad Tiltrotor eVTOL Vehicle," AIAA Scitech 2019 Forum, January, 2019, pp. 1–26.

[7] Johnson, W., "NDARC NASA Design and Analysis of Rotorcraft," NASA/TP-2015-218751, NASA, Moffett Field, CA, 2015.

[8] Lawrence, B., Theodore, C. R., Johnson, W., and Berger, T., "A Handling Qualities Analysis Tool for Rotorcraft Conceptual Designs," The Aeronautical Journal, Vol. 122, (1252), June 2018, pp. 960–987.

[9] Mills, B. and Datta, A., "Analysis of a Permanent Magnet Synchronous Motor Coupled to a Flexible Rotor for Electric VTOL," Annual Forum Proceedings - American Helicopter Society International, Vol. 2018-May, pp. 1–14.

[10] Sung, C. O. and Ali, E., "Test and Simulation of Axial Flux-Motor Characteristics for Hybrid Electric Vehicles," IEEE Transactions on Vehicular Technology, Vol. 53, No. 3, May 2004.

[11] Moreels, D., "Axial-Flux Motors and Generators Shrink Size, Weight," Power Electronics, Jul. 13, 2018.

[12] Aydin, M., Huang, S., and Lipo, T.A., "Axial Flux Permanent Magnet Disk Machines: A Review," Conf. Record of SPEEDAM, January 2004.

[13] Hincapie, J. S. L., Sandoval, A. V., and Parra, J. Z., "Axial Flux Electric Motor," Military University of New Granada. Mechatronics Engineering, 2012.

[14] Lambert, T., Biglarbegian, M.., and Mahmud, S., "A Novel Approach to the Design of Axial-Flux Switched-Reluctance Motors," *Machines* Vol. 3, No. 1, March 2015, pp. 27-54.

[15] Anonymous, "Technical Data and Manual for EMRAX Motors/Generators," EMRAX, Version 5.1, August 2018.

[16] Ivler, C., Niemiec, R., Gandhi, F. and Sanders, F. C., "Multirotor Electric Aerial Vehicle Model Validation with Flight Data: Physics-based and System Identification Models," Proceedings of the 75th Vertical Flight Society Annual Forum, Philadelphia, Pennsylvania, May 13-16, 2019.